

Numerical Modeling of Grain Structure in Continuous Casting of Steel

A.Z. Lorbiecka¹, R.Vertnik², H.Gjerkeš¹, G. Manojlović², B.Senčič²
J. Cesar² and B.Šarler^{1,3}

Abstract: A numerical model is developed for the simulation of solidification grain structure formation (equiaxed to columnar and columnar to equiaxed transitions) during the continuous casting process of steel billets. The cellular automata microstructure model is combined with the macroscopic heat transfer model. The cellular automata method is based on the Nastac's definition of neighborhood, Gaussian nucleation rule, and KGT growth model. The heat transfer model is solved by the meshless technique by using local collocation with radial basis functions. The microscopic model parameters have been adjusted with respect to the experimental data for steel 51CrMoV4. Simulations have been carried out for nominal casting conditions, reduced casting temperature, and reduced casting speed. Proper response of the multiscale model with respect to the observed grain structures has been proved.

Keyword: continuous casting of steel, solidification, multiscale modeling, equiaxed to columnar transition, columnar to equiaxed transition, macroscopic model, microscopic model, heat transfer model, cellular automata model, meshless methods.

1 Introduction

An important and huge class of manufacturing and materials processing operations include solidification of metals at some stage. Among these is the process of continuous casting of steel [Irwing, (1993)] most wide spread. The properties of the continuously cast billets, slabs and blooms in downstream processing are strongly

affected by the microstructural features and different types of defects, such as cracks, porosity and macrosegregation. There is a growing interest in computational modeling of continuous casting of steel [Thomas (2001); Šarler, Vertnik, Šaletić, Manojlović and Cesar (2005)], in order to be able to predict the properties of the product. The properties of the product can be calculated [Janssens, Raabe, Kozeschnik, Miodownik and Nestler (2007)] through a combination of the macroscopic and microscopic models. The macroscopic model calculates the relations between the process parameters and the macroscopic variables, such as temperatures, concentrations, and velocities on the scale of the process. The microscopic model calculates the relations between the macroscopic variables and the microstructure. The properties of the product can be related afterwards from the microstructure. The multiscale modeling [Shen and Atluri (2004); Haasemann, Kästner and Ulbricht (2006); Zhang and Shen (2008)] represents one of the currently most rapidly developing computational mechanics fields.

A principal goal of this study represents the development of a new simulation tool for modeling the dendritic grain structure in solidification of steel (equiaxed to columnar transition (ECT) and columnar to equiaxed transition (CET)) by using coupled micro and macroscopic models and validation of the model by experimental results. Several stochastic models of microstructure have been developed over the past years. The first approach was initiated by Spittle and Brown [Spittle and Brown (1989)], based on the Monte Carlo procedure to predict re-crystallization and grain growth in the solid – solid phase transformations, as well as to simulate the solidification structure. Rappaz and Gandin [Rappaz and Gandin (1993)]

¹ Laboratory for Multiphase Processes, University of Nova Gorica, Slovenia

² Štore Steel Company, d.o.o. Štore, Slovenia

³ Corresponding author. Email: bozidar.sarler@p-ng.si

were the first who applied another stochastic model, the Cellular Automata (CA) technique to predict solidification grain structure.

The present paper is structured in the following way: we present macroscopic and microscopic models first, followed by the description of the deterministic and stochastic solution procedures. The experimental validation of the model describes next. Finally, we represent the influence of the process parameters on the grain structure of the continuously cast billet.

2 Macroscopic model

The macroscopic model is designed to be able to calculate the steady temperature distribution in the continuously cast billet as a function of the following process parameters: billet dimension, steel grade, casting temperature, casting velocity, primary and two secondary cooling systems flows, pressures, temperatures, type and quantity of the casting powder, and the (non)application of the radiation shield and electromagnetic stirring. The Bennon-Incropera [Bennon and Incropera (1987)] mixture continuum formulation is used for the physical model, solved by the recently developed meshless Local Radial Basis Function Collocation Method (LRBFCM) [Šarler and Vertnik (2006); Vertnik and Šarler (2006); Vertnik, Založnik and Šarler (2006)]. In this novel numerical method, the domain and boundary of interest are divided into overlapping influence areas. On each of them, the fields are represented by the multiquadrics radial basis function collocation on a related sub-set of nodes. Time-stepping is performed in an explicit way. The governing equations are solved in its strong form, i.e. no integrations are performed. The polygonization is not present and the method is practically independent on the problem dimension. The other possibility represents the local approximation by the moving least squares [Šarler, Vertnik, Perko (2005)] instead of interpolation.

The convergence, continuity, and completeness of global radial basis function interpolation, based on the multiquadrics, has been recently elaborated by [Huang, Lee and Cheng (2007)]. A related comprehensive mathematical study is given

in [Buhmann (2003)]. At the present state-of-the-art, no rigorous mathematical theory exists for the local collocation. Nevertheless, the convergence of the method has been demonstrated for diffusion problems on NAFEMS [Cameron, Casey, Simpson (1986)] benchmark test and Dirichlet jump problem, and compared to the finite difference method (FDM) [Šarler and Vertnik (2006)]. The favorable convergence of the method compared to the classical second order FDM was demonstrated. The convergence of the LRBFCM was tested for convective-diffusive problems with and without phase change in [Vertnik and Šarler (2006)] and compared with the boundary element and finite element methods. Favorable convergence properties of the LRBFCM have been demonstrated in this case as well. The RBF-based numerical methods represent one of the key directions in meshless methods research for fluids [Amaziane, Naji and Ouazar (2004); Šarler (2005); Mai-Duy, Mai-Cao and Tran-Cong (2007); Divo and Kassab (2007); Kosec and Šarler (2008)], solids [Mai-Duy, Khennane and Tran-Cong (2007); Le, Mai-Dui, Tran-Cong and Baker (2008)], moving boundaries [La Rocca, Power, La Rocca and Morale (2005); Mai-Cao and Tran-Cong (2008)] and solution of partial differential methods in general [Mai-Duy and Tran-Cong (2003); Mai-Cao and Tran-Cong (2005)].

2.1 Governing equations

Consider a connected fixed domain Ω with boundary Γ occupied by a liquid-solid phase change material described with the temperature dependent density ρ_{φ} of the phase φ , temperature dependent specific heat at constant pressure c_{φ} , thermal conductivity k_{φ} , and the specific latent heat of the solid-liquid phase change h_m . The mixture continuum formulation [Bennon and Incropera (1987)] of the enthalpy conservation for the assumed system is

$$\frac{\partial}{\partial t}(\rho h) + \nabla \cdot (\rho \vec{v} h) = \nabla \cdot (k \nabla T) + \nabla \cdot (\rho \vec{v} h - f_S^V \rho_S \vec{v}_S h_S - f_L^V \rho_L \vec{v}_L h_L) \quad (1)$$

where the second term on the right-hand side is a correction term, needed to accommodate the

mixture continuum formulation of the convective term. In continuation we neglect this term. In Eq. (1) mixture density and thermal conductivity are defined as

$$\rho = f_S^V \rho_S + f_L^V \rho_L, \quad (2)$$

$$k = f_S^V k_S + f_L^V k_L, \quad (3)$$

where f_\varnothing^V represents the volume fraction of the phase \varnothing . The liquid volume fraction f_L^V might vary from 0 to 1 between solidus T_S and liquidus temperature T_L . Mixture velocity is defined as

$$\vec{v} = (f_S^V \rho_S \vec{v}_S + f_L^V \rho_L \vec{v}_L) / \rho, \quad (4)$$

and mixture enthalpy is defined as

$$h = f_S^V h_S + f_L^V h_L. \quad (5)$$

The constitutive temperature-enthalpy relationships are

$$h_S = \int_{T_{ref}}^T c_S dT, \quad (6)$$

$$h_L = h_S(T) + \int_{T_S}^T (c_L - c_S) dT + h_m, \quad (7)$$

with T_{ref} standing for the reference temperature. Thermal conductivity and specific heat of the phases can arbitrarily depend on temperature.

2.2 Spatial discretization

The temperature field of a point in the billet is prescribed by the following three-dimensional vector in the Cartesian coordinate system:

$$\mathbf{p} = xi_x + yi_y + zi_z, \quad (8)$$

where x, y, z are coordinates and $\mathbf{i}_x, \mathbf{i}_y, \mathbf{i}_z$ are base vectors. The z coordinate measures the length of the inner radius of the casting machine. This Cartesian coordinate system represents the flat geometry, which is the geometrical approximation of the real curved casting process (Fig. 1). The origin of the z coordinate coincides with the the top side of the mould, and the base vector \mathbf{i}_z coincides with the casting direction. The x coordinate measures the width (west-east direction) of the billet, perpendicular to the casting direction.

Its origin coincides with the centre of the billet. The y coordinate measures the thickness (south-north direction) of the billet, perpendicular to the casting direction. Its origin coincides with the inner (south) side of the billet.

According to the heat transfer phenomena of the continuous casting of steel, the heat conduction in the casting direction might be roughly neglected. The z coordinate is then parabolic, while the x and y coordinates are elliptic. The temperature field in the billet at a given time is described by the calculation of the cross-section (called infinite slice) temperature field of the billet. In this way the temperature field at a given z coordinate depends only on the slice history and its cooling intensity as a function of time. The slices form at the z_{start} longitudinal coordinate of casting and travel in the direction of the \mathbf{i}_z base vector with the casting speed v . For calculating the cooling intensity of the slice as a function of time, we need the connection between the z coordinate of the casting machine and the slice history t , which is in general

$$z(t) = \int_{t_{start}}^t v(t') dt' + z_{start}, \quad v(t) = \vec{v}(t) \cdot \mathbf{i}_z, \quad (9)$$

where t_{start} is the initial time of a slice. In the case when the casting speed and other process parameters are steady, we obtain the following simple connection between the z coordinate of the casting machine and the slice history t

$$t(z) = \frac{z - z_{start}}{v} + t_{start}. \quad (10)$$

$$\frac{\partial}{\partial t} (\rho h) = \nabla \cdot (k \nabla T). \quad (11)$$

In this paper, the simple Eq. (10) is used, since we assume the steady-state solution of the casting process. The prescribed simplified spatial discretization also simplifies the Eq. (1) by removing the convective terms. Thus the Eq. (1) transforms into transient equation, defined on x-y plane. This simplified model is consistent with the models, given by [Louhenkilpi (1995)].

2.3 Boundary conditions

The heat transport mechanisms in the mould take into account the heat transport mechanisms

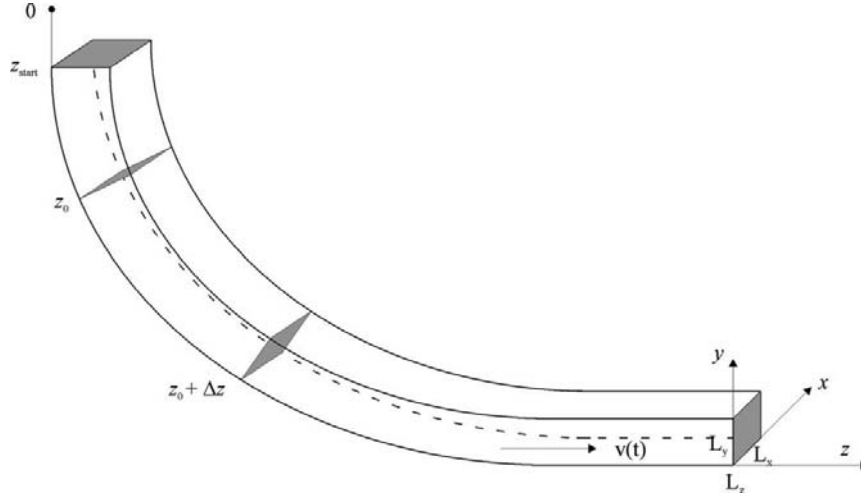


Figure 1: Slice traveling schematics of the billet (See Fig. 8 for the slice discretization).

through the casting powder, across the air-gap (if it exists), to the mould surface, in the mould, and from the mould inner surface to the mould cooling water. The heat transport mechanisms in the secondary cooling zone take into account the effects of the casting velocity, strand surface temperature, spray nozzle type, spray water flow, temperature and pressure, radiation and cooling through the rolls contact. Different types of the rolls are considered (driving, passive, centrally cooled, externally cooled, etc.). The mentioned basic heat transfer mechanisms are modified with regard to running water and rolls stagnant water at relevant positions. It is not possible to explicitly expose all the involved correlations within the scope of the present paper. Respectively, the calculated temperature distributions of the macroscopic model are given in Figs. 2-4 for the nominal conditions and for the reduced casting temperature and speed.

2.4 Solution procedure

We seek for mixture temperature at time $t_0 + \Delta t$ by assuming known initial temperature, velocity field, and boundary conditions at time t_0 . The initial value of the temperature $T(\mathbf{p}, t)$ at a point with position vector \mathbf{p} and time t_0 is defined through the known function T_0

$$T(\mathbf{p}, t) = T_0(\mathbf{p}); \mathbf{p} \in \Omega + \Gamma \quad (12)$$

The boundary Γ is divided into not necessarily

connected parts $\Gamma = \Gamma^D \cup \Gamma^N \cup \Gamma^R$ with Dirichlet, Neumann and Robin type boundary conditions, respectively. At the boundary point \mathbf{p} with normal \mathbf{n}_Γ and time $t_0 \leq t \leq t_0 + \Delta t$, these boundary conditions are defined through known functions $T_\Gamma^D, T_\Gamma^N, T_\Gamma^R, T_{\Gamma ref}^R$

$$T = T_\Gamma^D; \mathbf{p} \in \Gamma^D \quad (13)$$

$$\frac{\partial}{\partial n_\Gamma} T = T_\Gamma^N; \mathbf{p} \in \Gamma^N \quad (14)$$

$$\frac{\partial}{\partial n_\Gamma} T = T_\Gamma^R (T - T_{\Gamma ref}^R); \mathbf{p} \in \Gamma^R \quad (15)$$

The numerical discretization of Eq. (11), using explicit (Euler) time discretization has the form

$$\frac{\partial(\rho h)}{\partial t} \approx \frac{\rho h - \rho_0 h_0}{\Delta t} = \nabla \cdot (k_0 \nabla T_0) \quad (16)$$

From Eq. (16) the unknown function value h_l in domain node \mathbf{p}_l can be calculated as

$$h_l = h_{0l} + \frac{\Delta t}{\rho_0 c_0} (\nabla k_{0l} \cdot \nabla T_{0l} + k_{0l} \cdot \nabla^2 T_{0l}) \quad (17)$$

The spatial derivatives in Eq. (17) are approximated by the LRBFCM. In the LRBFCM, the representation of unknown function value over a set of lN (in general) non-equally spaced nodes $l\mathbf{p}_n$; $n = 1, 2, \dots, lN$ is made in the following way

$$\phi(\mathbf{p}) \approx \sum_{k=1}^{lK} l\psi_k(\mathbf{p})l\alpha_k \quad (18)$$

where ${}_l\psi_k$ stands for the shape functions, ${}_l\alpha_k$ for the coefficients of the shape functions, and ${}_lK$ represents the number of the shape functions. The left lower index on entries of expression (18) represents the influence domain (subdomain or support) ${}_l\omega$ on which the coefficients ${}_l\alpha_k$ are determined. The influence domains ${}_l\omega$ can in general be contiguous (overlapping) or non-contiguous (non-overlapping). Each of the influence domains ${}_l\omega$ includes ${}_lN$ nodes of which ${}_lN_\Omega$ can in general be in the domain and ${}_lN_\Gamma$ on the boundary, i.e. ${}_lN = {}_lN_\Omega + {}_lN_\Gamma$. The total number of all nodes \mathbf{p}_n is equal $N = N_\Omega + N_\Gamma$ of which N_Γ are located on the boundary and N_Ω are located in the domain. The influence domain of the node ${}_l\mathbf{p}$ is defined with the nodes having the nearest ${}_lN - 1$ distances to the node ${}_l\mathbf{p}$. The five noded ${}_lN = 5$ influence domains are used in this paper. The coefficients are calculated by the collocation (interpolation).

Let us assume the known function values ${}_l\phi_n$ in the nodes ${}_l\mathbf{p}_n$ of the influence domain ${}_l\omega$. The collocation implies

$$\phi({}_l\mathbf{p}_n) = \sum_{k=1}^{{}_lN} {}_l\psi_k({}_l\mathbf{p}_n) {}_l\alpha_k. \quad (19)$$

For the coefficients to be computable, the number of the shape functions has to match the number of the collocation points ${}_lK = {}_lN$, and the collocation matrix has to be non-singular. The system of Eqs. (19) can be written in a matrix-vector notation

$${}_l\psi {}_l\alpha = {}_l\Phi; \quad {}_l\psi_{kn} = {}_l\psi_k({}_l\mathbf{p}_n), \quad {}_l\phi_n = \phi({}_l\mathbf{p}_n). \quad (20)$$

The coefficients ${}_l\alpha$ can be computed by inverting the system (20)

$${}_l\alpha = {}_l\psi^{-1} {}_l\Phi. \quad (21)$$

By taking into account the expressions for the calculation of the coefficients, ${}_l\alpha$ the collocation representation of temperature $\phi(\mathbf{p})$ on subdomain ${}_l\omega$ can be expressed as

$$\phi(\mathbf{p}) \approx \sum_{k=1}^{{}_lN} {}_l\psi_k(\mathbf{p}) \sum_{n=1}^{{}_lN} {}_l\psi_{kn}^{-1} {}_l\phi_n. \quad (22)$$

The first partial spatial derivatives of $\phi(\mathbf{p})$ on subdomain ${}_l\omega$ can be expressed as

$$\frac{\partial}{\partial p_\zeta} \phi(\mathbf{p}) \approx \sum_{k=1}^{{}_lN} \frac{\partial}{\partial p_\zeta} {}_l\psi_k(\mathbf{p}) \sum_{n=1}^{{}_lN} {}_l\psi_{kn}^{-1} {}_l\phi_n; \quad \zeta = x, y. \quad (23)$$

The second partial spatial derivatives of $\phi(\mathbf{p})$ on subdomain ${}_l\omega$ can be expressed as

$$\frac{\partial^2}{\partial p_\zeta \partial p_\xi} \phi(\mathbf{p}) \approx \sum_{k=1}^{{}_lN} \frac{\partial^2}{\partial p_\zeta \partial p_\xi} {}_l\psi_k(\mathbf{p}) \sum_{n=1}^{{}_lN} {}_l\psi_{kn}^{-1} {}_l\phi_n; \quad \zeta, \xi = x, y. \quad (24)$$

The radial basis functions, such as multiquadrics, can be used for the shape functions

$${}_l\psi_k(\mathbf{p}) = [{}_l r_k^2(\mathbf{p}) + c^2]^{1/2}, \quad (25)$$

where c represents the shape parameter. These functions possess C^∞ continuity and can easily be used for approximation of the involved first and second order derivatives. The explicit values of the involved first and second derivatives of $\psi_k(\mathbf{p})$ are

$$\frac{\partial}{\partial p_\zeta} {}_l\psi_k(\mathbf{p}) = \frac{p_\zeta - {}_l p_{k\zeta}}{({}_l r_k^2 + c^2)^{1/2}}, \quad \zeta = x, y \quad (26)$$

$$\frac{\partial^2}{\partial p_\zeta^2} {}_l\psi_k(\mathbf{p}) = \frac{{}_l r_k^2 - (p_\zeta - {}_l p_{k\zeta})^2 + c^2}{({}_l r_k^2 + c^2)^{3/2}}, \quad \zeta = x, y \quad (27)$$

More elaborated step by step description and testing of the present solution procedure for temperature field is presented in [Šarler and Vertnik (2006)]. A successful comparison of the present meshless solution with the conventional CFD code Fluent for the continuous casting of steel is given in [Vertnik, Šarler, Buliński and Manojlović (2007)]. The use of the model in simulation system for continuous casting of steel billets is given in [Šarler, Vertnik, Gjerkeš, Lorbicka, Manojlović, Cesar, Marčič and Sabolič (2006)].

2.5 Macroscopic simulations

Simulations were performed for the billet of dimension 140x140 mm and the spring steel grade 51CrMoV4. The process parameters were taken directly from the process computer, installed on the casting machine.

The thermo-physical material properties of the spring steel were calculated by the JMatPro software [Saunders, Li, Miodownik and Schille (2003)]. Three simulations have been prepared for input of the microscopic model (see details in Tab. 1). The numerical results for each case are presented in Figs. 2-4, where the centerline and corner temperatures along the casting direction are plotted. In each figure, the top line represents the centerline temperature, the middle lines represent centerline temperatures of the surfaces, and the bottom lines represent the corner temperatures.

3 Microscopic model

The following three processes take place on the microstructure level:

- Nucleation process: occurs when a small grain of solid forms in the liquid. This is a kinetic process in which a small number of

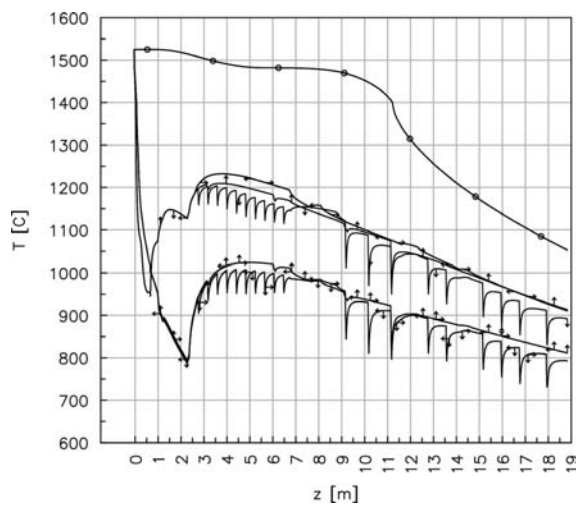


Figure 2: Centerline and corner temperatures along the casting direction. Nominal values (NOMINAL).

atoms form a stable cluster, called nucleus. The rate of nucleation depends mainly on the extent of the under-cooling.

- Growth process: once a grain nucleates it is going to increase its size since the atoms from the liquid are attaching to the tiny initial solid.
- Impingement: growth continues until the grains occupy the whole region, previously occupied by the liquid phase.

The present model is designed to be able to simulate the positions of the Equiaxed to Columnar Transition (ECT) and Columnar to Equiaxed Transformations (CET), see Fig. 9. A similar model has been already used for modeling the grain structure in aluminum-titanium alloys [Liu, Guo, Wu, Su and Fu (2006)]. The model is structured as follows.

3.1 Nucleation model

Two different assumptions [Lee and Hong (1997)] can be used for modeling of nucleation: a continuous dependency of nucleation density on temperature (i.e. under-cooling) or the instantaneous dependency of nucleation density on temperature. In the present study we adopted continuous nucleation model in which two different continuous nucleation modes were considered: at the surface area (index s) and in the bulk area (index b). The increase of grain density dn which corresponds to an under-cooling increase $d(\Delta T)$ can be modeled as follows

$$\left(\frac{dn}{d(\Delta T)} \right)_{\zeta} = \frac{n_{\max, \zeta}}{\sqrt{2\pi}\Delta T_{\sigma, \zeta}} \exp \left[-\frac{\overline{\Delta T} - \Delta T_{\max, \zeta}}{\Delta T_{\sigma, \zeta} \sqrt{2}} \right]^2, \quad \zeta := s, b \quad (28)$$

where: $\Delta T_{\max, s}$, $\Delta T_{\max, b}$, $\Delta T_{\sigma, s}$, $\Delta T_{\sigma, b}$, $n_{\max, b}$ and $n_{\max, s}$ represent the mean nucleation under-cooling at the surface area, the mean nucleation under-cooling in the bulk area, the standard deviation for the temperature at the surface area, the standard deviation for the temperature at the bulk area, and the maximum density of nuclei that can

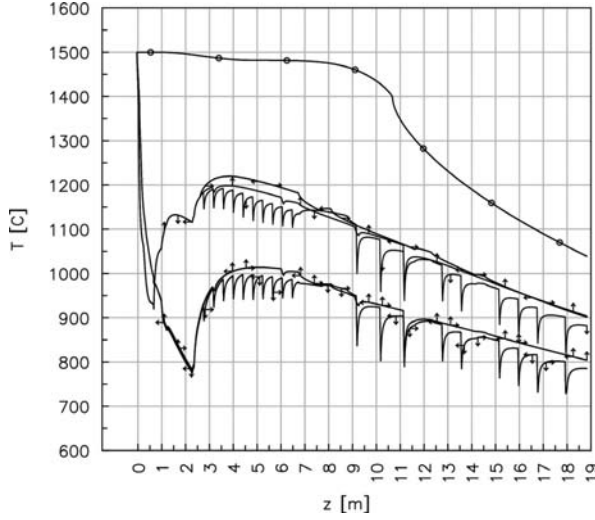


Figure 3: Centerline and corner temperatures along the casting direction. Reduced casting temperature (CASE I).

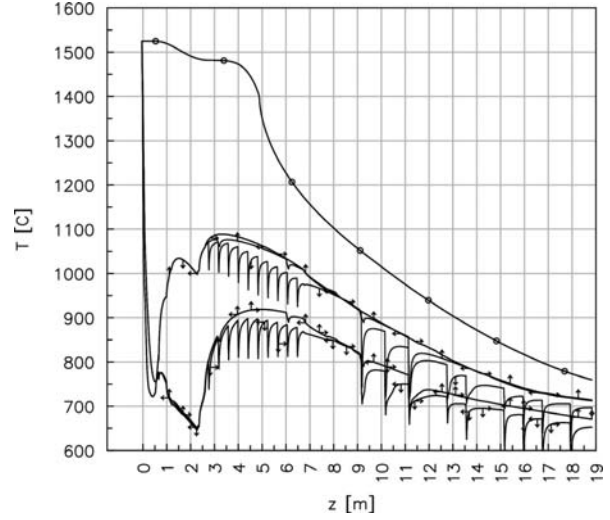


Figure 4: Centerline and corner temperatures along the casting direction. Reduced casting speed (CASE II).

Table 1: Nominal and varied process parameters of the 0.14 m billet casting of 51CrMoV4 steel. Varied process parameters are in bold.

	$T_{cast} (^{\circ}\text{C})$	$v_{cast} (\text{m/min})$
NOMINAL	1525	1,750
CASE I	1500	1,750
CASE II	1525	1,00

form in the melt for the surface and bulk, respectively. It is assumed that the highest occupancy of nucleuses is expected in the range of $(-3\Delta T_{\sigma}$ to $+3\Delta T_{\sigma})$, where ΔT_{σ} means standard deviation since the Gaussian distribution was chosen.

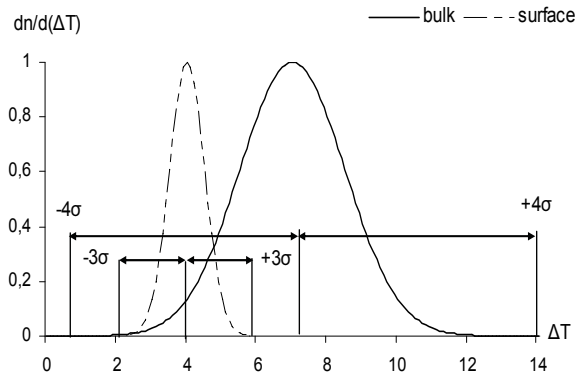


Figure 5: Nucleation curves for the surface and the bulk.

3.2 Growth model

The [Kurz, Giovanola and Trivedi (1986)] (KGT) model was used as the model of the growth kinetics. The growth velocity in each point is calculated through the following quadratic form

$$V^2A + VB + C = 0 \quad (29)$$

where the coefficients A , B and C are modeled as

$$A = \frac{\pi^2\Gamma}{\text{Pe}^2D^2}, \quad (30)$$

$$B = \frac{mC_0(1-k_0)\xi_c}{D[1-(1-k_0)\text{Iv}(\text{Pe})]}, \quad (31)$$

$$C = G, \quad (32)$$

with

$$\text{Iv}(\text{Pe}) = \exp(\text{Pe})\text{erfc}(\sqrt{\text{Pe}})\sqrt{\pi\text{Pe}},$$

$$\xi_c = \frac{\pi^2\Gamma}{k_0\text{Pe}}, \quad \text{Pe} = \frac{RV}{2D} \quad (33)$$

Where Γ , D , m , C_0 , k_0 , Pe , $Iv(Pe)$ and G are Gibbs-Thomson coefficient, diffusion coefficient in liquid, slope of the liquidus line, initial concentration of carbon, partition coefficient, Peclet number for solute diffusion, Ivantsov function, and temperature gradient, respectively. The temperature gradient G at a surface has little influence on the growth velocity and it was set to 0 ($G = 0$) as proposed by [Kurz, Giovanola and Trivedi (1986)] which reduces the equation (29) as follows: $V = -B/A$. The under-cooling in front of the dendrite tip was solved as follows [Kurz and Fisher (1998)]

$$\Delta T = m(C_0 - C_l) + \frac{2\Gamma}{r} \quad (34)$$

$$C_l = \frac{C_0}{1 - (1 - k_0)Iv(Pe)} \quad (35)$$

Where the dendrite tip radius r is expressed as

$$r = \sqrt{\frac{\Gamma D [1 - (1 - k_0)Iv(Pe)]}{-mV(1 - k_0)C_0}} \quad (36)$$

The under-cooling temperature ΔT was calculated through the assumed value of Peclet number Pe and through equations (35, 36). These results are related with the under-cooling temperatures ΔT received from the macro heat transfer calculation in order to calculate the growth velocity. To reduce the calculation effort, the values of growth velocity $V(Pe)$ and under-cooling temperature $\Delta T(Pe)$ were obtained in advance. The least squares method is used to obtain the coefficients a_1 , a_2 , a_3 of the growth velocity in the range of Pe numbers from 0.004 to 10 (with step 0.002)

$$V(\Delta T) = a_1(\Delta T)^3 + a_2(\Delta T)^2 + a_3(\Delta T) \\ a_i = (Pe, \Delta T); \quad i = 1, 2, 3 \quad (37)$$

The same assumption was also used by [Kurz, Giovanola and Trivedi (1986); Yamazaki, Natsume, Harada and Ohsasa (2006)]. If some of the assumed parameters from the growth process change, the coefficients in the relation $V(\Delta T)$ have to be changed as well.

3.3 Impingement model

At the beginning all calculation area is liquid. The nucleation process takes place in the mushy zone where the first grains nucleate. The process is completed until each of the grains completely touch his neighbors.

3.4 Numerical solution of microstructure equations

Microstructure equations are numerically solved by the CA technique [Rappaz, Bellet and Deville (2003)]. This method is associated with a system where the behavior is generated by predefined rules based on the local relationship between nearest neighboring cells, into which the domain is divided. Each cell has a 'state': liquid or solid and a 'neighborhood' configuration associated with it. The rules for evolution of the state of an individual cell within the CA system are in the present context already defined through the rules for nucleation, growth and impingement.

The only parameter which is varied during simulation is the value of local under-cooling ΔT , calculated from the macroscopic model. For each cell the nucleation conditions are checked: appropriate temperature ΔT in the micro cell and the probability condition. During each time step all cells are assigned a random number between ($0 < rand < 1$) and a random computational angle from $\langle (-45^\circ) - (+45^\circ) \rangle$. The transformation from liquid to solid will occur only when $rand < p$ where $p = \exp \left[(\Delta T - \Delta T_{max}) / (\sqrt{2}\Delta T_\sigma) \right]^2$. Once a cell is nucleated it grows with a preferential direction corresponding to its assigned crystallographic orientation and with respect to the heat flow. Depending on the randomly chosen angle the following neighborhood configurations [Nastac (2004)] (see Fig. 6) are chosen: Neumann, Moore and modified Moore respectively. All of new nucleuses which arise from the 'parent' grow with different randomly chosen configuration which is fixed for them at the time when they occur. For all „neighbours” of the treated nucleus, the criterion d is checked by using the for-

mula

$$d = l(t) / a_\theta, \quad l(t) = \int_{t_0}^t V(\Delta T) dt, \quad (38)$$

$$a_\theta = a\sqrt{\tan^2 \theta + 1},$$

where t , t_0 , a , θ and $l(t)$ are the actual time, initial time, the size of the cell, the crystallographic angle, and the length between the centre of the reference cell and its neighborhood cell, respectively. If a neighbor is one of the four nearest east, north, west, and south neighbors $a_\theta = a$ but if a neighbor is a corner neighbor then $a_\theta = a\sqrt{2}$. When $d \geq 1$, the growth front of the solid reference cell can touch the centre of the neighboring cell and then this cell transforms its state from liquid to solid [Zhu and Hong (2001)]. It is assumed that the growth is not allowed to take place for more than half of micro cell during each time step.

3.5 Coupling of the macroscopic and microscopic temperature fields

In this paper 4120 axial temperature fields were prepared from the macroscopic model. Each field has a dimension 14 x 14 cm and the size of each macro cell is 0.5 cm. There are 784 cells and 841 nodes of macro temperatures at each axial position. Macroscopic temperature field values have to be interpolated for use in the microscopic model. The temperature of a micro cell is influenced by its nearest neighboring macro calculation nodes T_i . The interpolation formula [Xu and Liu (2001)] used in the present work is

$$T_a = \left(\sum_{i=1}^4 T_i * w \right) / \sum_{i=1}^4 w, \quad w = \exp[-(l_i/2.8)] \quad (39)$$

Where T_a , T_i and l_i represents the temperature of the micro CA cell, the temperature of the neighboring macro nodes and the distance to the nearest macro nodes, respectively. Each macro cell is divided into 625 micro CA cells for the calculation of nucleation and grain growth. Obtained values of temperatures are recalculated into the under-cooling temperatures by using the following formula: $\Delta T = T_{liq} - T$ and then interpolated

for each micro cell during time. It was noticed that the grid size should be around 200 μm , because in this range the simulation results are stable and match the experiments. Two time-step loops are used in the program: macro loop with 0.3 s time step and micro loop with micro time step of 1.5 ms.

3.6 Calculation parameters of the microscopic model

The input data to the microscopic model has a tremendous influence on the final grain distribution. Respectively, a sensitivity study has been performed to study this influence and to adjust the model parameters to experimental values from Fig. 9. The input data of the microscopic solidification model are presented below, see Tab. 2.

The information connected with one cell (position in the domain, angle, CA configuration, time of generation), and all cells (amount of nucleuses, generated at the surface and in the bulk areas) are stored in a file for each micro time step. Simulations with different values show that changing some of the parameters can strongly affect the final appearance of microstructure. It can be observed, that the nucleation parameters of Gaussian distribution influence mostly the final grain structure. They determine the number of possible generated nucleuses at the surface and in the bulk area. By changing the range of ΔT_{\max} parameter the calculated area where new grains arise is widen. The changes of the parameters indirectly influence the probability condition and rapidly increase or decrease the amount of nucleated grains. It is shown [Lorbiecka and Šarler (2008)] that the best results, with respect to the experimental data, are received in the range of ΔT_σ from 1.25 K to 1.75 K for the bulk and around 0.2 K for the surface area. It was shown that the smaller casting velocity increases longer columnar forms what is seen on the examples. On the other hand, the higher casting temperature is, the more extended central zone becomes what is consistent with the measurements as well.

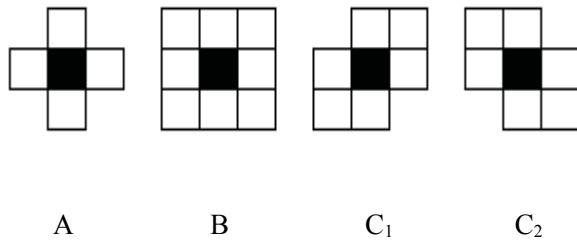


Figure 6: Definition of neighborhood configuration: A - Neumann, B - Moore, C₁ and C₂ - modified Moore respectively.

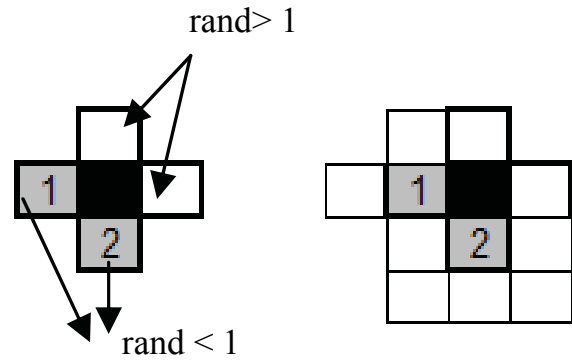


Figure 7: Schematics of the neighborhood.

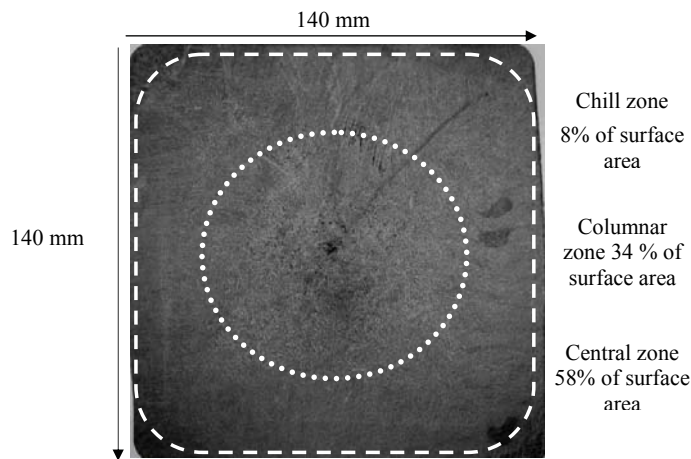


Figure 9: Observed (Baumann print) equiaxed to columnar (ECT) transition between chill and columnar zone (—) and columnar to equiaxed transitions (CET) between columnar and central zone (***) for the Nominal case.

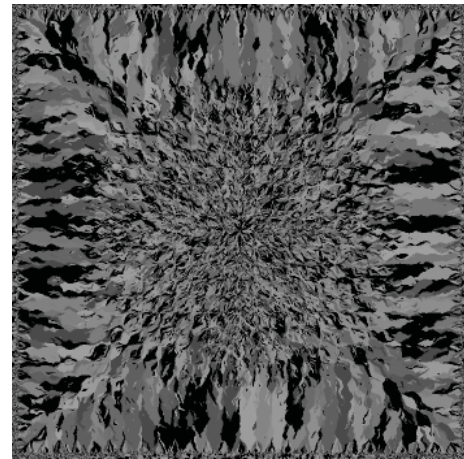


Figure 10: Simulated grain structure of the billet with ECT and CET.

4 Numerical implementation

Both, the macro and the micro models were coded in Fortran.

Macroscopic simulator takes about 3 minutes to prepare the macro temperature fields, while microscopic simulation takes approximately 6 hours on a standard PC with 3 Ghz and 1024 Ram. During the simulation the results can be observed on the screen, and afterwards post-processed. The described multiscale model was coupled only in the direction from macro to micro calculations. The results represent good match with the experiment, as elaborated in the next chapter.

5 Simulations of ECT and CET

A steel grade, used in this paper, has chemical composition 51CrMoV4. The simulated final microstructure (see Fig. 10), calculated with the nominal values from Tabs. 1 and 2. compare well with the experimental Baumann print, represented on Fig. 9. The macroscopic parameters have been subsequently varied, following the second and third row of Tab.1.

Table 3: Number of generated nucleuses for three simulated cases

Macro temp. filed	Nucleuses at surface	Nucleuses at bulk
CASE I	8543	15569
NOMINAL	14533	18200
CASE II	10609	10493

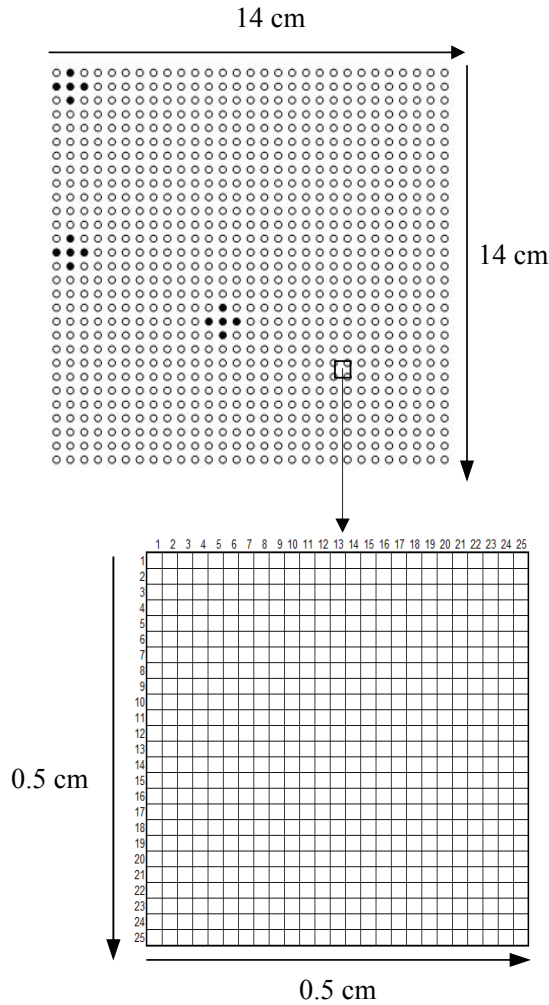


Figure 8: Relationship between macro field - meshless (above) and micro CA mesh (below). Solid circles in the macro field represent schematics of the corner, surface and bulk 5-noded domains of influence of the meshless method.

6 Conclusions

The coupled multiscale model was developed to predict the grain nucleation, growth and final structure (ECT and CET) of the continuously cast steel billets. The meshless LRBFCM was used to

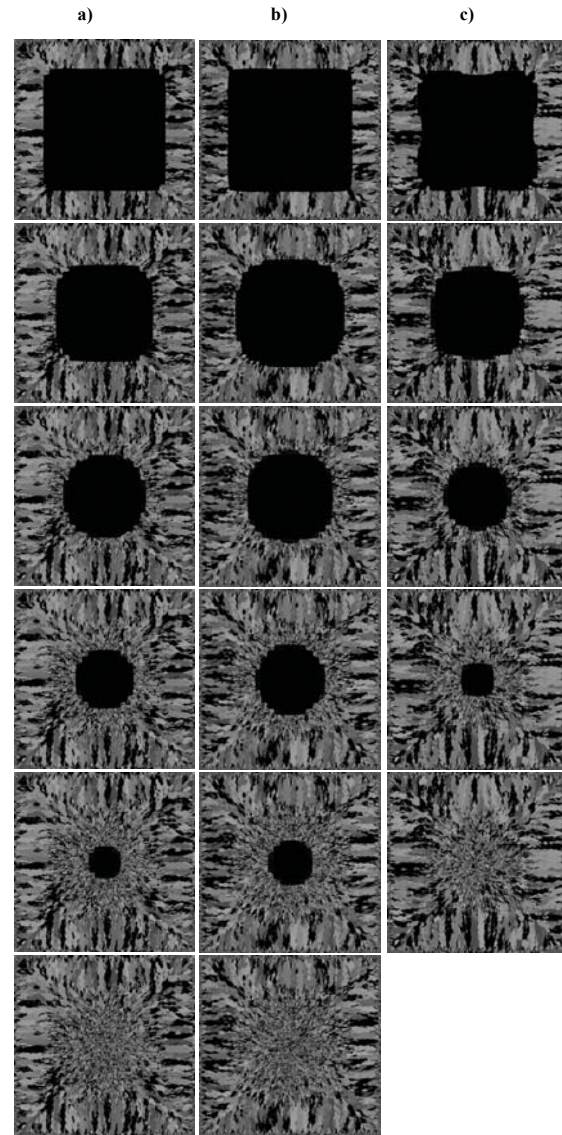


Figure 11: Calculated microstructures. a) $T_{cast}=1500\text{ }^{\circ}\text{C}$, $V_{cast}=1.75\text{ m/min}$ (CASE I) (from top to the bottom : 1min, 2min, 3min, 4min, 5min, 5 min 33s); b) $T_{cast}=1530\text{ }^{\circ}\text{C}$, $V_{cast}=1.75\text{ m/min}$ (NOMINAL) (from top to zhe bottom: 1min, 2min, 3min, 4min, 5min, 5 min 55s); c) $T_{cast}=1530\text{ }^{\circ}\text{C}$, $V_{cast}=1.00\text{ m/min}$ (CASE II) (from top to the bottom: 1min, 2min, 3min, 4min, 4 min 36 s).

Table 2: Nominal parameters used in the simulation.

Symbol	Value	Unit
$\Delta T_{\max, bulk}$	30.00	K
$\Delta T_{\max, surface}$	0.60	K
$\Delta T_{\sigma, bulk}$	1.75	K
$\Delta T_{\sigma, surface}$	0.20	K
k_0	0.370	1
Γ	$1.9 \cdot 10^{-7}$	Km
D	$2.0 \cdot 10^{-8}$	m^2/s
C_0	0.51	%
M	-30	1
a_1	$4,01 \cdot 10^{-3}$	1
a_2	$4,37 \cdot 10^{-3}$	1
a_3	$2,02 \cdot 10^{-4}$	1
T_{liq}	1755.01	K
T_{sol}	1672.04	K
V_{cast}	1.75	m/min
<i>micro cell size</i>	200	μm
<i>Surface area thickness</i>	0.5	cm

solve the macroscopic heat transfer model and the CA technique was used to solve the microstructure evolution. The model parameters were adjusted in order to obtain the experimentally determined actual billet ECT and CET positions for 51CrMoV4 spring steel.

The influence of the variation of the principal macroscopic heat transfer parameters (casting temperature and casting speed) on calculated grain structure was shown. Our future research will focus on inclusion of the variable concentration field in the model and implementation of irregular CA (transition from cell-wise description to point-wise description and transition from regular to irregular pointwise description) [Janssens (2000)]. Irregular CA involve the meshless philosophy also on the microscopic level. With this, the whole multiscale model would be able to be solved in a meshless [Atluri (2004); Liu and Gu (2005); Šarler (2007)] sense.

Acknowledgement: The first author would like to thank the European Marie Curie Research Training Network INSPIRE for position to study and research at the University of Nova Gorica,

Slovenia. Other authors wish to acknowledge the Slovenian Research Agency and Štore - Steel company for funding in the framework of the project L9-9508 Simulation of microstructure for steels with topmost quality.

References

- Amaziane, B.; Naji, A.; Ouazar, D.** (2004): Radial basis function and genetic algorithms for parameters identification to some groundwater flow problems, *CMC: Computers, Materials, & Continua*, vol. 1, pp.117-128.
- Atluri, S.N.** (2004): *The Meshless Method (MLPG) for Domain and BIE Discretization*, Tech Science Press, Forsyth.
- Bennon, W.D.; Incropera, F.P.** (1987): A continuum model for momentum, heat and species transport in binary solid-liquid phase change systems - I. Formulation. *International Journal of Heat and Mass Transfer*, vol. 30, pp. 2161-2170.
- Buhmann, M.D.** (2003): *Radial Basis Functions*, Cambridge University Press, Cambridge.
- Cameron, A.D.; Casey, J.A.; Simpson, G.B.** (1986): *Benchmark Tests for Thermal Analysis*, NAFEMS National Agency for Finite Element Methods & Standards, Department of Trade and Industry, National Engineering Laboratory, Glasgow.
- Divo, E.; Kassab, A.J.** (2007): An efficient localized RBF meshless method for fluid flow and conjugate heat transfer. *ASME Journal of Heat Transfer*, vol. 129, pp. 124-136.
- Haasemann, G.; Kästner, M.; Ulbricht, V.** (2006): Multi-scale modeling and simulation of textile reinforced materials, *CMC: Computers, Materials, & Continua*, vol. 3, pp. 131-146.
- Huang, C.S.; Lee, C.-F.; Cheng, A.H.-D.** (2007): Error estimate, optimal shape factor, and high precision computation of multiquadric collocation method, *Engineering Analysis with Boundary Elements*, vol. 31, pp. 614-623.
- Irwing, W.R.** (1993): *Continuous Casting of Steel*, The University Press Cambridge, Great Britain.
- Janssens, K.G.H.** (2000): Irregular cellular au-

tomato modeling of grain growth, In: Raabe, D.; Roters, F.; Barlat, F.; Chen, L.Q. (eds.) *Continuum Scale Simulation of Engineering Materials: Fundamentals – Microstructures - Process Applications*, Wiley-VCH, Germany, pp. 297-307.

Janssens, K.G.H.; Raabe, D.; Kozeschnik, E.; Miodownik, M.A.; Nestler, B. (2007): *Computational Materials Engineering*, Elsevier Academic Press, Great Britain, 2007.

Kosec, G.; Šarler, B. (2008): Local radial basis function collocation method for Darcy flow, *CMES: Computer Modeling in Engineering & Sciences*, vol.25, pp.197-207.

Kurz, W.; Giovanola, B.; Trivedi, R. (1986): Theory of microstructural development during rapid solidification, *Acta metall*, vol. 34, pp. 823-830.

Kurz, W.; Fisher D.J. (1998): *Fundamentals of solidification*, Trans. Tech. Publications Ltd, Switzerland.

La Rocca, A.; Power, H.; La Rocca, V.; Morale, M. (2005): A meshless approach based upon radial basis function hermite collocation method for predicting the cooling and freezing time of foods, *CMC: Computers, Materials, & Continua*, vol. 2, pp. 239-250.

Le, P.; Mai-Duy, N.; Tran-Cong, T.; Baker, G. (2008): A meshless modeling of dynamic strain localization in quasi-brittle materials using radial basic function networks, *CMES: Computer Modeling in Engineering & Sciences*, vol. 25, pp. 43-66.

Lee, K.Y.; Hong, C.P (1997): Stochastic modeling of solidification grain structure of Al-Cu crystalline Ribbons in Planar Flow Casting, *ISIJ International*, vol. 37, pp. 38-46.

Liu, G.R.; Gu, Y.T. (2005): *An Introduction to Meshfree Methods and Their Programming*, Springer, Dordrecht.

Liu, D.R.; Guo, J.J.; Wu, S.P.; Su, Y.Q.; Fu, H.Z. (2006): Stochastic modeling of columnar-to-equiaxed transition in Ti-(45-48at%) Al alloy ingots, *Materials Science and Engineering*, vol. A415, pp.184 -194.

Louhenkilpi, S. (1995): *Simulation and Control*

of Heat Transfer in Continuous Casting of Steel, Acta Polytechnica Scandinavica, Chemical Technology Series No. 230, The Finnish Academy of Technology, Finland.

Lorbiecka, A.; Šarler, B. (2008): A sensitivity study of grain growth model for prediction of ECT and CET transformations in continuous casting of steel, *Materials Science Forum*, (in print).

Mai-Cao, L.; Tran-Cong, T. (2005): A meshless IRBFN-based method for transient problems, *CMES: Computer Modeling in Engineering & Sciences*, vol. 7, pp. 149-171.

Mai-Cao, L.; Tran-Cong, T. (2008): A meshless approach to capturing moving interfaces in passive transport problems, *CMES: Computer Modeling in Engineering & Sciences*, vol. 31, pp. 157-188.

Mai-Duy, N.; Tran-Cong, T. (2003): Indirect RBFN method with thin plate splines for numerical solution of differential equations, *CMES: Computer Modeling in Engineering & Sciences*, vol. 4, pp. 85-102.

Mai-Duy, N.; Khennane, A.; Tran-Cong, T. (2007): Computation of laminated composite plates using integrated radial basis function networks, *CMC: Computers, Materials, & Continua*, vol. 5, pp. 63-78.

Mai-Duy, N.; Mai-Cao, L.; Tran-Cong, T. (2007): Computation of transient viscous flows using indirect radial basic function networks, *CMES: Computer Modeling in Engineering & Sciences*, vol. 18, pp. 59-77.

Nastac, L. (2004): *Modeling and Simulation of Microstructure Evolution in Solidifying Alloys*, Kluwer Academic Publishers, USA.

Rappaz, M.; Gandin, Ch.-A. (1993): Probabilistic modelling of microstructure formation in solidification processes, *Acta Metall. Mater.*, vol. 41, pp. 345-360.

Rappaz, M.; Bellet, M.; Deville, M. (2003): *Numerical Modelling in Materials Science and Engineering*, Springer Series in Computational Mechanics, Springer, Berlin.

Saunders, N.; Li, X.; Miodownik, P.; Schille, J.Ph. (2003): Using JmatPro to model materi-

als properties and behavior, *Journal of Metals*, vol.55, pp. 60-65.

Shen, S.; Atluri, S.N. (2004): Computational nano-mechanics and multi-scale simulation, *CMC: Computers, Materials, & Continua*, vol. 1, pp.59-90.

Spittle, J.A.; Brown, S.G.R (1989): Computer simulation of the effects of alloy variables on the grain structures of castings, *Acta Metall. Mater.*, vol. 37, pp. 1803-1810.

Šarler, B. (2005): A radial basis function collocation approach in computational fluid dynamics. *CMES: Computer Modeling in Engineering & Sciences*, vol. 7, pp. 185-193.

Šarler, B.; Vertnik, R.; Perko, J. (2005): Application of diffuse approximate method in convective diffusive solidification problems, *CMC: Computers, Materials, & Continua*, vol. 2, pp. 77-83.

Šarler, B.; Vertnik, R. (2006): Meshfree local radial basis function collocation method for diffusion problems. *Computers and Mathematics with Application*, vol. 51, pp. 1269-1282.

Šarler, B.; Vertnik, R.; Gjerkeš, H.; Lorbiecka, A.; Manojlović, G.; Cesar, J.; Marčič, B.; Sabolič, M. (2006): Multiscale integrated numerical simulation approach in Store - Steel cast-house. *WSEAS Transactions on Systems and Control*, vol. 1, pp.294-299.

Šarler, B.; Vertnik, R.; Šaletiš, S.; Manojlović, G.; Cesar, J. (2005): Application of continuous casting simulation at Štore Steel. *Berg- und Hüttenmännische Monatsheft*, invol. 150, pp. 300-306.

Šarler, B. (2007): From global to local radial basis function collocation method for transport phenomena, *Advances in Meshfree Techniques*, Springer, Berlin, pp. 257-282.

Thomas, B.G. (2001): Continuous casting: modeling, In: J. Dantzig, A. Greenwell, J. Michalczuk, (eds) *The Encyclopedia of Advanced Materials*, Pergamon Elsevier Science, Oxford, United Kingdom.

Vertnik, R.; Šarler, B. (2006): Meshless local radial basis function collocation method for

convective-diffusive solid-liquid phase change problems. *International Journal of Numerical Methods for Heat & Fluid Flow*, vol. 16, pp. 617-640.

Vertnik, R.; Založnik, M.; Šarler, B. (2006): Solution of transient direct-chill aluminium billet casting problem with simultaneous material and interphase moving boundaries by a meshless method. *Engineering Analysis with Boundary Elements*, vol. 30, pp. 847-855.

Vertnik, R.; Šarler, B.; Buliški, Z.; Manojlović, G. (2007): Solution of transient temperature field in continuous casting of steel by a meshless method. In: Andreas, L. (ed) *2nd International Conference of Simulation and Modelling of Metallurgical Processes in Steelmaking, Steelsim 2007*, ASMET, Leoben, Austria, pp. 223-228.

Xu, Q.Y.; Liu, B.C. (2001): Modeling of as-cast microstructure of Al alloy with a modified cellular automaton method, *Materials Transactions*, vol. 42, pp. 2316-2321.

Yamazaki, M.; Natsume, Y.; Harada, H.; Ohsasa, K. (2006): Numerical simulation of solidification structure formation during continuous casting in Fe-0.7mass%C alloy using cellular automaton method, *ISIJ International*, vol. 46, pp. 903-908.

Zhang, Y.; Shen, S. (2008): A modified multiscale model for microcantilevel sensor, *CMC: Computers, Materials, & Continua*, vol. 8, pp. 17-22.

Zhu, M.F.; Hong, C.P. (2001): A modified cellular automaton model for the simulation of dendritic growth in solidification of alloys, *ISIJ International*, vol. 41, pp. 436-445.